Test particle transport from long-range collisions*

F. Anderegg†, X.-P. Huang,[a] E. M. Hollmann, C. F. Driscoll, T. M. O'Neil, and D. H. E. Dubin
Institute for Pure and Applied Physical Sciences and Department of Physics, University of California at San Diego, La Jolla, California 92093

(Received 11 November 1996; accepted 14 January 1997)

Enhanced cross-magnetic-field diffusion of test particles in pure ion plasmas has been measured. The ion plasma is contained in a Penning-Malmberg trap for weeks near thermodynamic equilibrium, characterized by rigid rotation and uniform density and temperature. Plasma expansion and loss is suppressed by a ''rotating wall'' technique, i.e., a weak electrostatic potential rotating faster than the plasma. Test particle transport is then measured even though there is zero net transport, in a regime where neutral collisions are negligible. The observed test particle transport is diffusive, i.e., proportional to the gradient of the test particle concentration. The measured diffusion coefficients scale as $nT^{-1/2}B^{-2}$ over a range of 40 in density, 50 in temperature, and 5 in magnetic field. This diffusion is about ten times greater than predicted by classical collisional theory, which describes velocity-scattering collisions with impact parameters $\rho \lesssim r_c$. The enhanced transport is thought to be due to non-velocity-scattering ''**E×B** drift'' collisions with $r_c < \rho \lesssim \lambda_D$. Initial estimates of diffusion due to these long-range collisions are three times less than the measurements, and substantial theory questions remain. © *1997 American Institute of Physics.* [S1070-664X(97)92505-2]

I. INTRODUCTION

Cross-magnetic-field test particle transport is an active area of plasma theory and experiment; important questions are collisions versus wave-induced, and the range of the interaction. Classical Boltzmann theory describes ion transport in terms of short-range velocity scattering collisions, with impact parameters less than the cyclotron radius $\rho < r_c$. Long-range ''**E×B** drift'' collision theory considers impact parameters $r_c < \rho \lesssim \lambda_D$. Obviously, in a non-neutral plasma where $\lambda_D > r_c$ (due to the Brillouin limit), long-range interactions may play an important role. Also, they may be important for heat transport in a neutral plasma where the cyclotron radius of the electron is $r_{ce} < \lambda_D$.

Experimentally, there has been substantial effort to measure test ion cross-magnetic field transport. In the field of basic plasma physics, important progress has been made after the principle demonstration of optical tagging of ions by Stern *et al.*[1] Experiments using optical tagging show classical diffusion of ions in a Q-machine.[2] Fasoli *et al.*[3] changed background pressure to modify the distribution function $f(v)$ and explained the measured test-particle transport in terms of classical diffusion with a B^{-2} scaling of the diffusive process. They also suggest that in the presence of shear parallel flow, the diffusion process may be replaced by convection.[4]

In fusion plasmas, measurements of tritium particle transport have been reported by Efthimion *et al.*,[5] with tritium density inferred from the neutron emissivity. They calculate tritium fluxes as functions of time, thus obtaining diffusion and convection coefficients. They found that the convective term is generally small; but a direct comparison of the diffusion coefficient with theory is difficult due to the complexity of the fusion device.

Other work focuses on velocity-space diffusion, often referred to as Fokker-Planck diffusion. Experimental work performed in Q-machines and gas discharge have shown reasonable agreement with the predictions of Fokker-Planck theory.[6] A special case is the measurement of the anisotropic temperature relaxation in a magnetized pure electron plasma,[7] which was found to be in precise agreement with Fokker-Planck theory. One secondary result of the present research is to establish that collisional temperature isotropization in pure ion plasmas is quantitatively predicted by Fokker-Planck theory.

According to theory, bulk transport (as opposed to test-particle diffusion) may be greatly enhanced by long range interactions; even though the effect of long range **E×B** drift collision is subtle on the diffusion of test particles, it can lead to orders of magnitude increase in the viscosity and change the magnetic field scaling. According to calculations[8] based on Boltzmann theory, the viscosity scales as B^{-4}, while as long range **E×B** drift collisions[9] predict B^{-2}, and long range two-dimensional (2D) interaction theory[10] scales as B^{-1}. Measurement of bulk viscous transport in pure electron plasmas scales[11] as B^{-1}.

We report in this paper experiments to quantify these long-range collisional interactions in a quiescent magnesium ion plasma contained in a Penning-Malmberg trap[12] near thermal equilibrium. Bulk plasma expansion is suppressed by a weak ''rotating wall,'' i.e., an electrostatic potential on the wall rotating faster than the plasma.[13] Test particle transport is then measured even though there is zero net transport. Ions are tagged by spin orientation, and the slow cross field

*Paper 5IA2, Bull. Am. Phys. Soc. **41**, 1477 (1996).
†Invited speaker.
[a]Present address: Time and Frequency Division, NIST, Boulder, Colorado 80303.

 1070-664X/97/4(5)/1552/7/$10.00

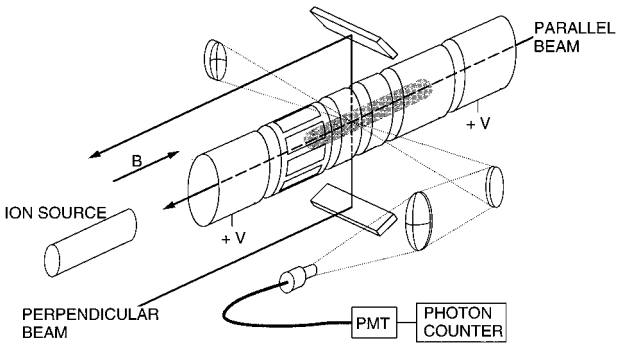

FIG. 1. Schematic diagram of the cylindrical ion trap, with perpendicular and parallel laser beams and LIF detector. A ''rotating wall'' drive applied to the segmented electrode gives steady-state confinement.

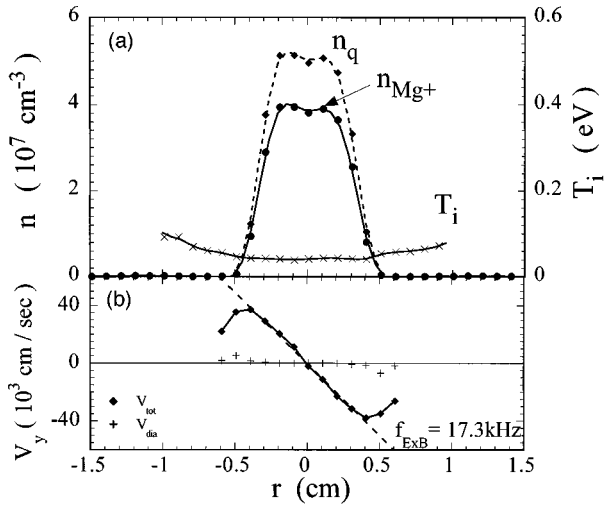

FIG. 2. (a) Measured Mg^+ density $n(r)$ and temperature $T(r)$, with inferred total charge density $n_q(r)$. (b) Measured fluid rotation $V_{\rm tot}(r)$ and calculated diamagnetic rotation rate $V_{\rm dia}$.

diffusion of these test particles is accurately measured using Laser Induced Fluorescence (LIF).

The measured diffusion is about ten times greater than predicted by classical theory of diffusion due to velocity-scattering collisions.[14] Further, the scaling is the same except for small logarithmic corrections: the measured diffusion coefficients scale approximately as $nT^{-1/2}B^{-2}$ over a range of 40 in density n, 50 in temperature T, and 5 in magnetic field B. Simultaneous measurements of thermal isotropization establish that velocity-space scatterings are not anomalously large.

This enhanced diffusion is probably due to long-range ''**E×B** drift'' collisions. Present calculations of this enhanced test-particle diffusion are about three times larger than classical, i.e., three times smaller than the measurements. However, the diffusion from these long-range collisions depends on long-time correlations between the positions of individual ions, and thus is quite sensitive to small effects which perturb the ion trajectories. We believe that further theory effort is required to fully understand these subtle collisions.

II. APPARATUS

The cylindrically symmetric ion trap is shown schematically in Fig. 1. The electrodes are contained in an ultra-high vacuum chamber $P=3\times10^{-9}$ Torr (97% H_2). The ions are created by a metal vacuum vapor arc source (MEVVA),[15] then injected into the trap by lowering briefly the positive potential of one end cylinder. Free electrons are ejected axially. Radial confinement is provided by a uniform magnetic field ($B\leqslant 4$ T) created by a superconductive coil, which by itself would give a plasma loss time of $\tau_L\leqslant 2000$ s. The losses are essentially suppressed by applying a ''rotating wall'' signal to eight insulated wall patches.[13] This rotating field, varying as $e^{im\theta-i\omega t}$ with $m=1$, adds angular momentum and energy to the plasma, balancing the drag and energy loss from magnetic field asymmetries and collisions with neutrals. The inside electrode radius is $R_w=2.86$ cm; the plasma dimensions are typically 0.4 cm $\leqslant r_p\leqslant$0.9 cm and $L_p\simeq 10$ cm. Typically, 3×10^8 ions are confined for weeks.

The central electrode has been cut out to let a laser beam perpendicular to the magnetic field intersect the plasma. Side holes (not shown in Fig. 1) allow the laser induced fluorescence to be detected from the perpendicular or parallel beam.[16]

A continuous (CW) laser was chosen based on signal-to-noise considerations and for optimum velocity resolution. Transition from the ground state $3s^2S_{1/2}$ to the lowest excited states ($3p^2P_{1/2}$ or $3p^2P_{3/2}$) of a Mg^+ ion are in the 280 nm range. Such wavelengths are obtained by frequency doubling of a CW ring dye laser. We use a Bergquist scheme:[17] A nonlinear crystal (Beta Barium Metaborate ''BBO,'' 3 mm $\times$3 mm $\times$5 mm) in an external doubling cavity converts the tuneable beam (560 nm, $\leqslant$1 W) into an ultraviolet beam (280 nm, $\leqslant$20 mW) with a bandwidth of 1 MHz. The ring doubling cavity is stabilized by a feedback loop using an error signal created by a polarized sensitive detector.

The plasma density, temperature, and rotation velocity profiles are obtained from a $\sim$0.5 mW beam which is scanned across the plasma, with a detection volume of 1 mm$^2\times$3 mm ($\Delta x\Delta z\Delta y$). At each radial position, the frequency of the laser is scanned 60 GHz across a $3^2S_{1/2}\rightarrow 3^2P_{3/2}$ ''cyclone'' transition of Mg^+ in 1.7 s, giving 141 frequency bins of 10 ms with a 2 ms dwell time between each bin. This gives the θ-averaged ion velocity distribution; and the density $n(r)$, temperature $T(r)$, and total rotation velocity $v_{\rm tot}(r)$ are obtained by fitting to a shifted Maxwellian distribution. This weak diagnostic beam applies negligible torque on the plasma. The plasma is near-Maxwellian, since perturbations are weak compared to the ion-ion velocity scattering rate $\nu_{ii}\equiv(16\sqrt{\pi}/15)\times nb^2\overline{v}\ln(r_c/b)\approx(0.1/{\rm s})T^{-3/2}(n/10^6)$, where $\overline{v}\equiv(T/M)^{1/2}$, $b\equiv e^2/T$, and $r_c\equiv\overline{v}/(eB/Mc)$.

Figure 2 shows density, temperature, and rotation velocities for an ion plasma that has been confined for 22 hours with $B=4$ T. We estimate the total confined charge density as $n_q(r)=\alpha n(r)$, with α obtained from the measured rotation velocity. Specifically, we fit $v_{\rm tot}(r)=(c/B)[E(r)-\nabla(nT)/ne]$ with $\nabla\cdot E(r)=4\pi e n_q(r)$. As can be seen from Fig. 2, the diamagnetic term is quite small at low tem-

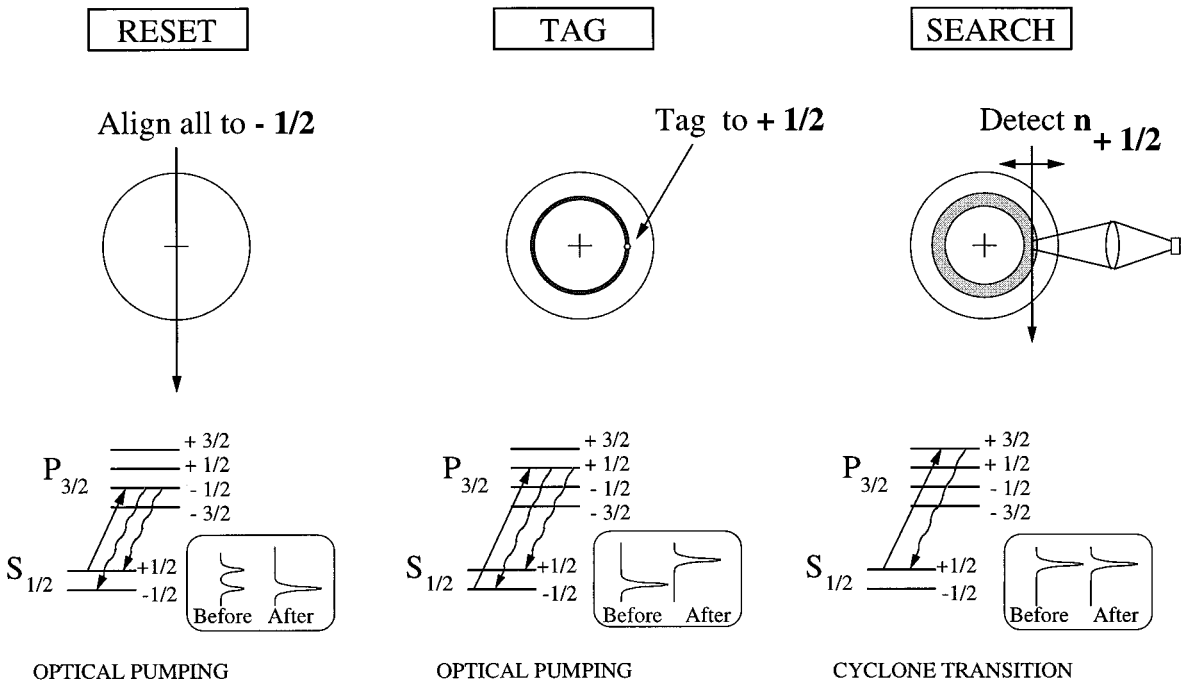

FIG. 3. The three steps used to measure test particle transport. First all spins are aligned parallel to B ($M_j=-1/2$); then test particles are locally ''tagged'' to $M_j=+1/2$; finally test particles are non-destructively detected. Also shown are the relevant energy levels of Mg^+.

peratures, so the total fluid rotation velocity is close to the **E×B** rotation velocity, and determination of α is straightforward. For $T>10^{-2}$ eV, there is negligible centrifugal separation of the ion species present in the trap.[18] For this plasma, about 75% of the charge is Mg^+, with MgH_n^+ probably constituting most of the remainder. The ion plasma has axial length $L_p\approx 10$ cm, and individual ions bounce axially at a rate $f_b\equiv \overline{v}/2L_p\approx 3$ kHz for average thermal energy $T=0.1$ eV.

The ion plasmas tend to cool to about 0.05 eV due to collisions with neutrals, as shown in Fig. 2. We can increase the ion temperature either by ion cyclotron resonance heating[19] from an $m=1$ voltage applied to wall sectors, or by compressional heating from an $m=0$ voltage applied to an end cylinder. Both techniques were used in the data presented here, with no noticeable differences in the resulting test particle transport.

The ion spin orientation is used to ''tag'' the test particles. Electronic ion spin orientation has been shown to be a robust technique to label test particles.[20] The ground state of Mg^+ is a $3^2S_{1/2}$ state. In a magnetic field, the spin orientation can be $M_j=+1/2$ or $-1/2$; and the difference of energy between these two states is very small (4.6×10^{-4} eV at 4 T). Nevertheless, measurements indicate that the ion spin polarization is robust, degrading with a time constant $10^4<\tau_s<10$ s for 0.05 eV $\leqslant T\leqslant$ 5 eV. This is longer than the time required for the tagged ions to diffuse radially.

Three steps are used to measure test particle transport; they are graphically represented in Fig. 3.

(A) Reset. The plasma is completely polarized into the $S_{1/2}^{M_j=-1/2}$ state by direct optical pumping with a beam tuned to $S_{1/2}^{M_j=+1/2}\rightarrow P_{3/2}^{M_j=-1/2}$ transition. This beam is perpendicular to the magnetic field and passes through the center of the plasma. It is left on for a long time (10 s) to ensure that all ions have passed through the beam due to their bounce and rotation motion and interact resonantly with it.

(B) Tag. The spin of particles at a chosen radial position r_t is reversed by direct optical pumping with a parallel beam tuned to $S_{1/2}^{M_j=-1/2}\rightarrow P_{3/2}^{M_j=+1/2}$. The tagging beam is left on for many rotations of the plasma and also for many bounce periods to ensure that most ions are pumped; typically 50 ms are required to locally tag more than 80% of ions into the $S_{1/2}^{M_j=+1/2}$ state.

(C) Search. The density of tagged particles at a chosen search position, $n_t(r_s,t)$, is measured non-destructively with a perpendicular beam tuned to the peak of the ''cyclone'' transition $S_{1/2}^{M_j=+1/2}\rightarrow P_{3/2}^{M_j=+3/2}$ which decays only to $S_{1/2}^{M_j=+1/2}$. This transition does not change (to first order approximation) the population of the states which are being probed. However, ''sideband'' excitation of other transitions due to the Lorentzian wings of the laser frequency spectrum will create optical pumping. This effect is crucial for laser cooling experiments,[21] but unwanted in our case. To avoid it, the search beam is weak and is on less than 10% of the time; also, high magnetic field helps to minimize sideband pumping.

III. RESULTS

The test particle density n_t is recorded as a function of time at a fixed search radius r_s; Fig. 4 shows n_t at $r_s=-0.52$ cm versus time t, from just after the tagging to 15 s. The time $t=0$ is defined as when the 50 ms tagging pulse starts. For each data point, the LIF signal is measured for 40 ms at the peak of the distribution function. From a

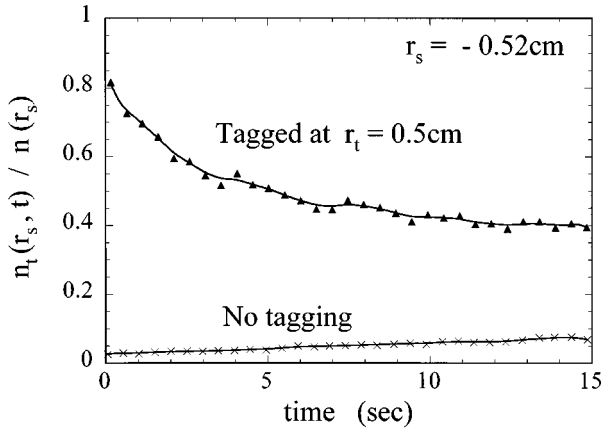

FIG. 4. Concentration of test particles n_t/n versus time at search position $r_s=-0.52$ cm; the tag beam was located at $r_t=0.5$ cm. Also shown is n_t/n in the absence of tagging, showing slow spin flip from collisions and sideband pumping.

regular LIF frequency scan determining $T(r)$ and the nonresonant background, the LIF data is then converted to $n_t(r_s,t)$. Also shown in Fig. 4 are the $\times$'s representing a case where no ions have been tagged, indicating the weak effect of spontaneous spin flips and sideband pumping. This measurement allows us to determine a rate of spin depolarization τ_s, which will be used later in Eq. (1) to correct for this unwanted effect.

The experiment cycle (Reset-Tag-Search) is repeated for 31 positions r_s, giving $n_t(r,t)$. Figure 5 shows three test particle profiles $n_t(r,t)$ at $t=$ 50 ms, 6 s, and 15 s visually showing radial diffusion towards $n_t/n=$constant; here, the tagging beam position was $r_t=$ 0.5 cm.

From the measured quantities $n(r)$, $T(r)$, $n_t(r,t)$, τ_s, the fluxes of test particles Γ_t can be calculated as

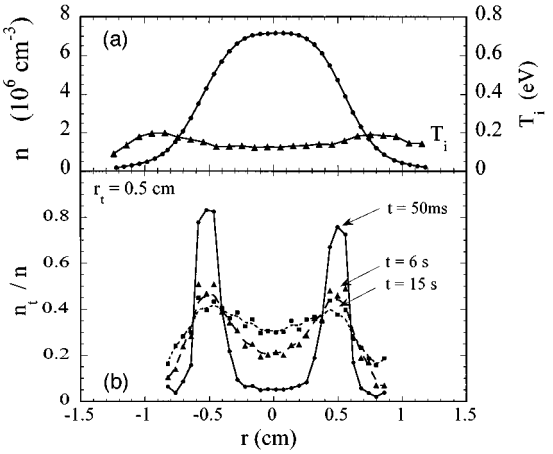

FIG. 5. (a) Measured density $n(r)$ and temperature $T(r)$ from collisions and for the heated plasma used in Figs. 4–7. (b) Measured test particle density $n_t(r,t)/n(r)$ at three times, showing radial diffusion towards n_t/n =constant.

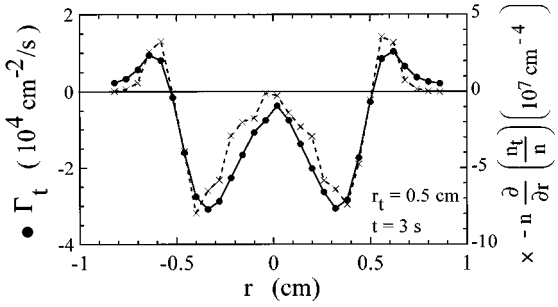

FIG. 6. Flux $\Gamma_t(r)$ and gradient $-n\partial/\partial r\ (n_t/n)$ at $t=3$ s; the two curves have similar radial dependence, showing flux proportional to the gradient.

$$\Gamma_t(r,t)=-\frac{1}{r}\int_0^r dx x\frac{\partial}{\partial t}n_t(x,t)+\int_0^r dx x\frac{2n_t(x,t)-n(x)}{\tau_s(x)}. \tag{1}$$

The second term corrects for the slow spontaneous spin flips at the separately measured rate τ_s^{-1}. With this correction, the total number of tagged particles is conserved to within 10%. This flux is then compared to a transport model including both local diffusion coefficient $D(r)$ and θ-averaged radial convection velocity $V_r(r)$:

$$\Gamma_t(r,t)=-D(r)n(r)\frac{\partial}{\partial r}\frac{n_t(r,t)}{n(r)}+V_r(r)n_t(r,t). \tag{2}$$

The diffusion term of Eq. (2) is proportional to the relative concentration of test particles n_t/n; this can be obtained from the rigorous two-species derivation of Longmire and Rosenbluth (Ref. 22). There will be no flux of test particles when the test particles are fully mixed and n_t/n has no gradient, even though n_t and n will still have gradients.

Figure 6 shows the radial dependence of the flux $\Gamma_t(r,t=3$ s) and the gradient $n(r)\partial/\partial r\ (n_t(r)/n(r))$. Both curves exhibit the same radial dependence, indicating that the flux Γ_t is proportional to the gradient of the relative

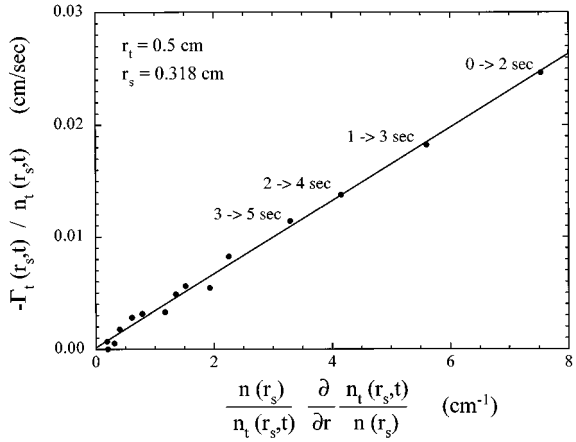

FIG. 7. Measured normalized test particle flux Γ_t/n_t versus normalized test particle gradient $(n/n_t)(\partial/\partial r)(n_t/n)$, showing Fick's law of diffusion, for the evolution of Figs. 4–7.

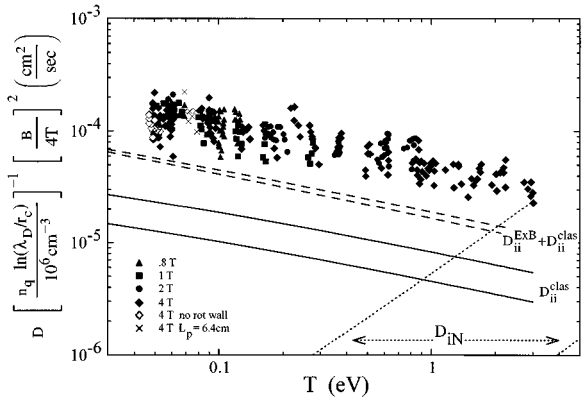

FIG. 8. Measured test particle diffusion coefficients D normalized to $n_q B^{-2}\ln(\lambda_D/r_c)$ versus temperature T. Theory curves show classical diffusion D_{ii}^{class}, estimates of $\mathbf{E\times B}$ drift diffusion $D_{ii}^{\mathbf{E\times B}}$, and diffusion from neutral collisions D_{iN}, for the range of densities observed.

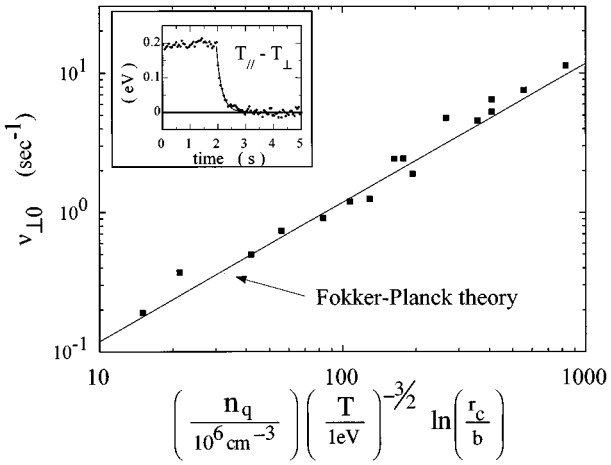

FIG. 9. Measured velocity-space isotropization rate $\nu_{\perp 0}$ compared to the prediction of theory, with no adjustable parameters. The insert shows a typical $T_\parallel - T_\perp$ measurement, with anisotropy maintained until $t=2$ s, then exponential relaxation to $T_\parallel = T_\perp$.

concentration of test particles $(\partial/\partial r\, n_t/n)$. Note that the data for Figs. 4–7 come from a single data set from tagging with $r_t = 0.5$ cm and $B = 4$ T.

Figure 7 shows the measured normalized flux Γ_t/n_t versus the measured normalized gradient $(n/n_t)(\partial/\partial r)(n_t/n)$ for one particular radius $r_s = 0.318$ cm. The different points represent different times in the evolution. The straight line fit to the data gives $D(r_s) = 3.3\times 10^{-3}$ cm^2/s and $V_r(r_s) = -1.4\times 10^{-4}$ cm/s. We obtain $V_r(r) = 0$ to experimental accuracy; this is to be expected, since these test particles are transported exactly the same as all other ions, and the total density $n(r)$ is independent of time, with no bulk radial flow. Similarly, with $n_t/n \equiv \beta g(r)$, Eq. (2) shows that Γ_t/n_t depends only on the profile $g(r)$ but not the absolute magnitude β; therefore Eq. (2) is valid even for $n_t/n = O(1)$. Figure 7 shows normalized flux proportional to normalized gradient over a range of 20 (Fick's law), indicating that higher powers of the gradient are not important here. Note that $(r-\theta)$ convective cells in the plasma column would still show $V_r(r) = 0$, due to the θ-averaged nature of the measurement, but could give a deviation from the straight line on Fig. 7 due to the non-locality of the process. However, convective cells would exhibit different density, temperature, and magnetic field scaling than that for collisional diffusion described below.

Figure 8 shows the measured diffusion coefficients D for densities 1×10^6 cm$^{-3} < n < 4\times 10^7$ cm^{-3} (from different r_s and from different plasmas), for $0.05 < T < 3$ eV (from auxiliary heating), and for magnetic fields $0.8 < B < 4$ T. The diffusion coefficients are normalized by $n_q B^{-2}\ln(\lambda_D/r_c)$, for comparison to classical and $\mathbf{E\times B}$ drift collisional theories described below. Over a wide range of temperatures, the data is about ten times greater than expected from classical collisions alone (D_{ii}^{class} shown by solid lines). This enhanced diffusion does not seem to be caused by the ''rotating wall,'' which keeps the ion cloud in steady-state: the open symbols of Fig. 8 were obtained with the rotating wall signal turned off during the test particle evolution. The ''rotating wall'' is balancing weak bulk transport due to field asymmetries and collisions with neutral atoms, which occurs on a ''loss'' time scale of $\tau_L \sim 1000$ s, whereas the measured test particle transport times are 1 s to 30 s. We thus believe that the rotating wall fields are too weak to have a significant influence on test particle transport.

IV. ANALYSIS

Classical transport theory describes steps in the position of an ion guiding center due to collisional scattering of the ion velocity vector, arising from binary ion-ion collisions with impact parameters ρ in the range $b < \rho < r_c$. Here $b \equiv e^2/T = (1.44\ \text{nm})T^{-1}$ is the classical distance of closest approach, and $r_c \equiv \overline{v}/\Omega_c = (500\ \mu\text{m})T^{1/2}B^{-1}$ is the cyclotron orbit radius. The predicted classical diffusion coefficient is[22]

$$D_{ii}^{\text{class}} = \frac{5}{4}\left(\frac{16\sqrt{\pi}}{15} n b^2 \overline{v}\ln\Lambda\right) r_c^2 \equiv \frac{5}{4}\nu_{ii} r_c^2 . \tag{3}$$

Here $\nu_{ii} \approx (0.10\ \text{s}^{-1})T^{-3/2}(n/10^6)$ is the ion-ion momentum-transfer collision rate, with Coulomb logarithm $\ln\Lambda = \ln(r_c/b)$ for a magnetized plasma,[23] giving $D_{ii}^{\text{class}} \approx (3.1\times\ 10^{-4}\ \text{cm}^2/\text{s})T^{-1/2}B^{-2}(n/10^6)$. The range of D_{ii}^{class} scaled by $[n_q \ln(\lambda_D/r_c)]^{-1}B^2$ is shown by the solid curves in Fig. 8; the range arises from the $\ln(\lambda_D/r_c)$ normalization which is not in classical theory. Of course, classical ion velocity scatterings from ion-neutral collisions can also give ion diffusion, but this coefficient $D_{iN} \approx \nu_{iN} r_c^2 \approx (2.4\times 10^{-4}\ \text{cm}^2/\text{s})(T^{1/2}+0.5)TB^{-2}$ is negligible at low pressure and temperature (dotted lines). Here, the second term is due to the fact that the neutrals are not at rest and that they are presumed to be H_2; the contribution due to the plasma rotation is negligible. Also, D_{iN} does not depend on the ion density and has very different temperature scaling.

This enhanced test particle diffusion is observed even though measurements of velocity-space isotropization in these plasmas agree closely with classical theory. We have induced anisotropies between $T_\parallel$ and $T_\perp$, and measured the relaxation of $T_\parallel(t)$ and $T_\perp(t)$ to a common final temperature T. Collisional theory predicts $(d/dt)(T_\perp - T)$

$= -\nu_{\perp 0}(T_\perp - T)$, with relaxation rate $\nu_{\perp 0} = 1.5\nu_{ii} = 3\nu_{\perp\|}$. Figure 9 shows the measured velocity scattering rates $\nu_{\perp 0}$ and the Fokker-Planck prediction,[7] with no adjustable parameters. Thus, there are no anomalously large velocity-scattering collisions causing the enhanced test-particle diffusion. Experimentally, this result also indicates that the density calibration is correct.

Long-range "**E×B** drift" collisions[9,24] with impact parameters ρ in the range $r_c < \rho < \lambda_D$ are the most likely explanation for the enhanced test particle diffusion. Two ions on field lines separated by $\Delta r \lesssim \lambda_D$ with small relative axial velocity will interact for a long time, and will **E×B** drift due to their mutual interaction field, even though there is no significant scattering of the velocity vectors. A simple estimate of the drifts evaluated on unperturbed orbits gives a diffusion coefficient

$$D_{ii}^{\mathbf{E\times B}} = 2\sqrt{\pi} n b^2 \overline{v} \overline{r_c^2} \ln\left(\frac{\lambda_D}{r_c}\right) \ln\left(\frac{\overline{v}}{\Delta v_z}\right). \tag{4}$$

The minimum relative axial velocity Δv_z that can be sustained by two ions is limited by velocity-scattering collisions and by rotational shear.[9] Diffusion of v_z from small-angle scatterings gives $(\Delta v_z)^2 = \nu_{ii}\overline{v^2}\tau$, and the interaction time τ is set by $(\Delta v_z)\tau \approx \lambda_D$, giving $\overline{v/}\Delta v_z \approx (\omega_p/\nu_{ii})^{1/3}$. Alternately, shear in the cross-field drift motion of ions separated radially by λ_D may limit the interaction time, giving $\overline{v/}\Delta v_z \approx (2\lambda_D/r_c)|f_E/r(\partial/\partial r)f_E|$.

An estimate for $D_{ii}^{\mathbf{E\times B}} + D_{ii}^{\text{class}}$ with Δv_z limited by collisions is shown by the two dashed lines on Fig. 8. Since the density enters Eq. (4) as $n\ln(n^{-1/2})$, it can not be completely scaled out in Fig. 8, and the two dashed curves represent the density extremes of the data, i.e., $n = 1\times 10^6$ cm^{-3} and 4×10^7 cm^{-3}. For these plasmas the shear limitation is generally negligible. The enhancement of the diffusion due to these long-range collisions is proportional to $\ln(\lambda_D/r_c)$; thus, at low magnetic field and large density, $D_{ii}^{\mathbf{E\times B}}$ may be smaller than D_{ii}^{class}. Since ions may "**E×B** collide" for longer than an axial bounce time, the diffusion could depend on the plasma length; the ×'s in Fig. 8 are for shorter plasmas, suggesting that end effects are not important in the enhanced diffusion.

The magnetic field dependence of the enhancement in diffusion is shown in Fig. 10. Here, we have subtracted D_{ii}^{class} from the measured D, and normalized the difference by $T^{-1/2} n_q \ln(\lambda_D/r_c)\ln(\overline{v/}\Delta v_z)$, where $\ln(\overline{v/}\Delta v_z)$ is taken to be limited by collisions. The normalized difference is then fit to αB^β, giving $\alpha = (1.0\pm 0.2)\times 10^{-4}$ and $\beta = -1.9\pm 0.1$; for comparison, Eq. (4) gives $\alpha = 3.67\times 10^{-5}$ and $\beta = -2$. Thus, the magnetic field dependence of the enhanced diffusion is consistent with estimates of Eq. (4) for long-range **E×B** drift collisions, but the amplitude given by Eq. (4) is too small by a factor of 2.7, as was also seen in Fig. 8.

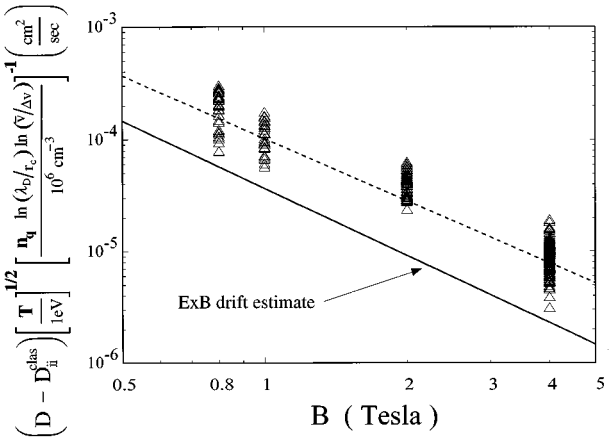

FIG. 10. Magnetic field scaling of the enhancement in measured diffusion coefficient D, scaled for comparison to theory. The dashed line shows the best fit to the data scaling as $B^{-1.9}$, and the solid line is the theory estimate of Eq. (4).

V. DISCUSSION

Measurements of the cross-field transport of test particles in a quiescent steady-state pure ion plasma have given quantitative diffusion coefficients over a range of 50 in temperature, 40 in density, and 5 in magnetic field. The measured diffusion coefficients are about ten times greater than predicted by classical collision theory, whereas the measured velocity-scattering collision frequency agrees closely with the prediction of Fokker-Planck theory.

An estimate of diffusion from long-range **E×B** drift collisions is roughly a factor of three less than the measured diffusion. We note that the collision integrals have been evaluated only to lowest order in $[\ln(\overline{v/}\Delta v)]^{-1}$ and $[\ln(\lambda_D/r_c)]^{-1}$; thus the estimate for $D_{\text{ii}}^{\mathbf{E\times B}}$ may be inaccurate by factors of 2 since the logarithms are in the range 2 to 5. Also, there is reason to believe that the integration along unperturbed orbits used to obtain Eq. (4) is inadequate, and that an improved analysis of the orbit integrals would yield a larger diffusion coefficient. This analysis is in progress.

Long-range interactions may give substantially larger enhancement to other transport coefficients, such as viscosity or heat conduction. The bulk viscous transport of ions would presumably be governed by an equation such as

$$\Gamma_{\text{bulk}}(r,t) = \frac{c}{eB}\frac{1}{r^2}\frac{\partial}{\partial r} r^2 \eta r \frac{\partial}{\partial r}\frac{v_{\text{tot}}(r,t)}{r} + V_r(r,t)n(r,t).$$

Here, the flux Γ_{bulk} is driven by collisional viscosity η acting on shears in the azimuthal fluid velocity $v_{\text{tot}} = (c/B)\times[E_r(r) - \nabla(nT)/ne]$. The radial convection V_r represents non-viscous transport, and would be zero in steady state. Since viscosity scales as $\eta \approx nm\nu_{ii}\overline{\rho^2}$, the average range $\overline{\rho}$ of the collisional interaction is crucial: $\overline{\rho} \propto \lambda_D$ for **E×B** drift collisions, whereas $\overline{\rho} \propto r_c$ for velocity-scattering collisions. Thus, theory suggests[9] that $\Gamma_{\text{bulk}} \propto B^{-2}$ for **E×B** drift collisions, in contrast to the Boltzmann prediction[8] of $\Gamma_{\text{bulk}} \propto B^{-4}$. In the regime where $\overline{v/}L_p \gg f_{\mathbf{E\times B}}$, a 2D (i.e., bounce-averaged) treatment of long-range collisions[10] gives an effective collision frequency $\nu_{\text{ii}}^{\text{eff}} \propto B^1$, resulting in $\Gamma_{\text{bulk}} \propto B^{-1}$.

These strong scaling differences are why long-range interactions give a rather subtle factor-of-10 enhancement in the test particle diffusion of Eq. (4), but give enhancement of 10^4–10^6 in bulk viscous transport. Experiments on pure electron plasmas[11] have shown $\Gamma_{\text{bulk}} \propto B^{-1}$, consistent with 2D long-range interactions. Indeed, the present ion experiments

are an attempt to quantify and further characterize this process. For heat transport, less is known experimentally and theoretically about the effect of long-range drift collisions, but we believe this will be a fruitful area of research.

ACKNOWLEDGMENTS

One of us (F.A.) thanks Dr. J. C. Bergquist for advice on laser frequency doubling. The technical support of R. Bongard is acknowledged.

This work was supported by Office of Naval Research Grant No. N00014-96-1-0239 and National Science Foundation Grant No. PHY94-21318.

[1]R. A. Stern, D. N. Hill, and N. Rynn, Phys. Lett. A **93**, 127 (1983).
[2]R. McWilliams and M. Okubo, Phys. Fluids **30**, 2849 (1987).
[3]A. F. Fasoli, F. N. Skiff, T. N. Good, P. J. Paris, and M. Q. Tran, IEEE Trans. Plasma Sci. **PS-20**, 655 (1992); A. F. Fasoli, F. N. Skiff, T. N. Good, and P. J. Paris, Phys. Rev. Lett. **68**, 2925 (1992).
[4]F. N. Skiff and A. F. Fasoli, Phys. Lett. A **184**, 104 (1993).
[5]P. C. Efthimion, L. C. Johnson, J. D. Strachan, E. J. Synakowski, M. Zarnstorff, H. Adler, C. Barnes, R. V. Budny, F. C. Jobes, M. Louglin, D. McCune, D. Mueller, A. T. Ramsey, G. Rewoldt, A. L. Roquemore, W. M. Tang, and G. Taylor, Phys. Rev. Lett. **75**, 85 (1995).
[6]J. Bowles, R. McWilliams, and N. Rynn, Phys. Plasma **1**, 3814 (1994); J. Curry, F. Skiff, M. Saffary, and T. Good, Phys. Rev. Lett. **74**, 1767 (1995).
[7]A. Hyatt, C. F. Driscoll, and J. H. Malmberg, Phys. Rev. Lett. **59**, 2975 (1987); S. Ichimaru and M. N. Rosenbluth, Phys. Fluids **13**, 2778 (1970).
[8]T. M. O'Neil and C. F. Driscoll, Phys. Fluids **22**, 266 (1979).
[9]T. M. O'Neil, Phys. Rev. Lett. **55**, 943 (1985).
[10]D. H. E. Dubin and T. M. O'Neil, Phys. Rev. Lett. **60**, 1286 (1988).
[11]C. F. Driscoll, J. H. Malmberg, and K. S. Fine, Phys. Rev. Lett. **60**, 1290 (1988).
[12]See, for example, *Non-Neutral Plasma Physics II*, edited by J. Fajans and D. Dubin, AIP Conf. Proc. 331 (American Institute of Physics, New York, 1995).
[13]X.-P. Huang, F. Anderegg, E. M. Hollmann, C. F. Driscoll, and T. M. O'Neil, Phys. Rev. Lett. **78**, 875 (1997).
[14]F. Anderegg, X.-P. Huang, C. F. Driscoll, E. M. Hollmann, T. M. O'Neil, and D. H. E. Dubin, Phys. Rev. Lett. **78**, 2128 (1997).
[15]R. A. MacGill, I. G. Brown, and J. E. Galvin, Rev. Sci. Instrum. **61**, 580 (1990).
[16]F. Anderegg, X.-P. Huang, E. Sarid, and C. F. Driscoll, ''A new pure ion plasma device with LIF diagnostic,'' submitted to Rev. Sci. Instrum.
[17]J. C. Bergquist, H. Hemmati, and W. Itano, Opt. Commun. **43**, 437 (1982).
[18]T. M. O'Neil, Phys. Fluids **24**, 1447 (1981).
[19]E. Sarid, F. Anderegg, and C. F. Driscoll, Phys. Plasmas **2**, 2895 (1995).
[20]F. Skiff, T. N. Good, F. Anderegg, and P. J. Paris, Phys. Lett. A **137**, 57 (1989).
[21]D. J. Wineland, J. C. Bergquist, W. M. Itano, and R. E. Drullinger, Opt. Lett. **5**, 245 (1980).
[22]C. L. Longmire and M. N. Rosenbluth, Phys. Rev. **103**, 507 (1956); L. Spitzer, *Physics of Fully Ionized Gas* (Interscience, New York, 1955).
[23]D. Montgomery, G. Joyce, and L. Turner, Phys. Fluids **17**, 2201 (1974).
[24]E. M. Lifshitz and L. P. Pietaefski, *Physical Kinetics* (Pergamon, New York, 1981), Sec. 60.